



## Article

# Spinnability and Morphological Stability of Carboxymethyl Cellulose and Poly(Vinyl Alcohol) Blends by Electrospinning

Javier M. Anaya-Mancipe <sup>1,2,\*</sup> , Vanessa F. da Silva <sup>1</sup>, Angela Y. Becerra-Lovera <sup>2</sup>, Marcos L. Dias <sup>2</sup>   
and Rossana M. S. M. Thiré <sup>1,\*</sup> 

<sup>1</sup> Program of Metallurgical and Materials Engineering—PEMM/COPPE, Universidade Federal do Rio de Janeiro (UFRJ), Rio de Janeiro 21941-599, Brazil

<sup>2</sup> Macromolecules Institute Professor Eloisa Mano—IMA, Universidade Federal do Rio de Janeiro (UFRJ), Rio de Janeiro 21941-598, Brazil; mldias@ima.ufrj.br (M.L.D.)

\* Correspondence: javier.anaya@metalmat.ufrj.br (J.M.A.-M.); rossana@metalmat.ufrj.br (R.M.S.M.T.); Tel.: +55-(21)-99558-9414 (J.M.A.-M.); +55-(21)-99604-5696 (R.M.S.M.T.)

**Abstract:** Carboxymethyl cellulose (CMC) is a plant-derived polymer known for its excellent anti-adhesive properties, making it suitable for dressings for highly exudative lesions. However, CMC alone is considered an un-spinnable biopolymer due to its complex intermolecular interactions. This study explored the spinnability of CMC through electrospinning by blending it with poly(vinyl alcohol) (PVA) at an 8:2 (PVA/CMC) ratio. Two types of PVA with varying molecular weights and degrees of hydrolysis were used at different concentrations. Solutions were prepared with Milli-Q water at 90 °C for about 2 h, followed by electrospinning under different voltages and flow rates. Scanning electron microscopy (SEM) was used to assess spinning ability, while Fourier-transform infrared spectroscopy (FTIR-ATR) characterized the mats' chemical composition. Thermal behavior was analyzed using thermogravimetry analysis (TGA) and differential scanning calorimetry (DSC). Results showed that the neat PVA.1 solution produced smaller nanofibers (~217.9 nm), while the PVA.1/CMC blend resulted in a smaller fiber diameter (129.9 nm) but with more defects due to higher surface tension. In contrast, PVA.2 and PVA.2/CMC exhibited larger diameters (448.6 nm and 270.1 nm, respectively) and better thermal and morphological stability, indicating their potential for anti-adhesive chronic wound dressings.

**Keywords:** carboxymethyl cellulose; electrospinning; nanofibers; morphology; wound dressing



**Citation:** Anaya-Mancipe, J.M.; da Silva, V.F.; Becerra-Lovera, A.Y.; Dias, M.L.; Thiré, R.M.S.M. Spinnability and Morphological Stability of Carboxymethyl Cellulose and Poly(Vinyl Alcohol) Blends by Electrospinning. *Processes* **2024**, *12*, 2759. <https://doi.org/10.3390/pr12122759>

Academic Editor: Maria Victoria López Ramón

Received: 1 November 2024

Revised: 20 November 2024

Accepted: 3 December 2024

Published: 4 December 2024



**Copyright:** © 2024 by the authors. Licensee MDPI, Basel, Switzerland. This article is an open access article distributed under the terms and conditions of the Creative Commons Attribution (CC BY) license (<https://creativecommons.org/licenses/by/4.0/>).

## 1. Introduction

Wound dressings based on carboxymethylcellulose (CMC) are known for their flexibility, high exudate absorption capacity, promotion of angiogenesis, and autolytic debridement [1,2]. CMC is widely used due to its non-toxic nature; it is water soluble and abundantly available in nature. It serves as the basis for many medications and materials implanted or used in the human body. As a result of these advantages, CMC-based biomaterials (hydrogels, films, nanocomposites) are extensively employed for wound dressings and drug delivery applications [3–6].

CMC is one of the most widely used cellulose-derived polymers in the industry. It is a cream-colored powder primarily used in the food industry, pharmaceuticals, detergents, and coatings [7]. Its most common form is as a sodium salt ( $\text{CH}_2\text{COONa}$ ). In this form, sodium carboxymethyl groups are attached to the hydroxyl group of the glucopyranose chain of the cellulose molecule. These side groups are responsible for the hydrophilic nature of CMC, in contrast to its precursor, cellulose [8,9].

However, one of the main disadvantages of CMC is its difficulty in processing using conventional methods. This is due to its strong hydrogen bonds, which result in low plasticity and a helical conformation in solution, significantly influencing the rheological behavior of CMC solutions. Such materials undergo thermal decomposition before reaching

their melting temperature [10]. The presence of specific chain conformations, hydrodynamic responses, and repulsive forces between the polyanions of natural polymers like CMC limits its practical applications and makes the electrospinning process challenging for many researchers [11]. Nevertheless, some researchers have successfully electrospun CMC using other easily spinnable polymers as support, such as PEO and PVP, among others [12–15].

Poly(vinyl alcohol) (PVA) is one of the most widely used polymers in skin dressing applications due to its water solubility, which allows its use in burns or wounds that produce high levels of exudate [16,17]. This property enables it to maintain moist environments that favor tissue regeneration.

PVA is a synthetic, semi-crystalline, hydrophilic, water-soluble polymer characterized by a simple chemical structure that includes hydroxyl (OH) side groups resulting from the alkaline hydrolysis of poly(vinyl acetate) (PVAc). The literature links the degree of hydrolysis to the fundamental properties of PVA, which affect the polymer's solubility, crystallinity, and surface tension in solution. PVAs with 100% hydrolysis exhibited greater hydrophilicity but lower water solubility [18,19]. Conversely, the presence of residual acetate groups results in weaker hydrogen bonds between and/or within chains compared to 100% hydrolyzed PVA. This weakening of hydrogen bonds between adjacent hydroxyl groups in PVA increases water solubility and decreases the melting temperature of the polymer [20].

For dressing applications, Jatoi et al. (2018) developed PVA nanofibers loaded with silica spheres containing silver nanoparticles anchored to the surface [21]. PVA nanofibers were electrospun using water as a solvent and glutaraldehyde as a crosslinking agent, resulting in fibers with an average diameter of approximately 170 nm for pure PVA and 277 nm for PVA with 15% mass of nanoparticles. The study demonstrated effective antimicrobial activity against *E. coli* and *S. aureus*, showing significant inhibition zones in plate studies, suggesting a promising methodology for biomedical applications, including wound dressings.

Elhaleem et al. (2020) utilized electrospun PVA nanofibers as a carrier matrix for cefotaxime, an antibacterial drug used in clinical settings [22]. However, this drug has a limited shelf life, which restricts its applicability. Therefore, the sustained release of encapsulated cefotaxime directly onto the burn was studied to prevent the proliferation of both Gram-negative and Gram-positive bacterial colonies, a significant issue in second-degree burns. A study in rats demonstrated that the application of these biomaterials promoted complete healing of the epithelial layer, indicating that the antimicrobial activity provided by the drug was crucial for an efficient healing process. However, the authors noted that for dressing applications, pure PVA presented some deficiencies due to its inadequate elasticity and hydrophobicity, recommending its use in dressings made from blends with polysaccharides and/or synthetic materials that enhance the biocompatibility of the blend, such as collagen and cellulose [23].

Oliveira et al. (2024) [24] studied the PVA and CMC blend as hydrogel carriers for phytopharmaceuticals and its influence on skin wounds, evaluating its swelling capacity as a model for exudate adsorption. The release of natural extracts from the studied hydrogels demonstrated effective behavior in delivering the different phytopharmaceuticals, particularly the flavonoids present in the secondary metabolites, which are characteristic substances of the various natural extracts. This indicates that this PVA/CMC polymer blend is capable of localized drug delivery to different skin wounds while hydrating the wound bed, thus promoting tissue repair—a characteristic feature of hydrocolloids like CMC.

A significant study on this blend was conducted by Cen et al. (2024) [25], who successfully synthesized a CMC from natural 1,3- $\beta$ -glucan (CU), a component capable of promoting the healing of diabetic wounds. This CMC was electrospun using PVA as a spinning support at a ratio of 1:4. Solutions varying in the concentration of native CU and its derivatives with PVA were electrospun to produce nanofiber mats with homogeneous diameters. The obtained samples were characterized to evaluate their potential in the regeneration of diabetic skin wounds in animal models, demonstrating a survival rate exceeding

90% in mice after three injections of STZ. This investigation highlights the amplified healing potential of electrospun PVA/CMC matrices compared to other electrospun blends of CU derivatives in diabetic wounds.

Electrospinning is one of the most widely employed methodologies for producing biomaterials for tissue regeneration and/or wound dressing applications [26]. This is primarily attributed to the submicrometric fibrillar structure of the mats, which mimics the natural structure of the extracellular matrix (ECM) of tissues [27]. Additionally, the properties offered by these nanostructures as biomaterials yield a high surface-to-mass ratio and high porosity, allowing for fluid exchange and the permeability of damaged tissues to the surrounding environment [28,29].

Thus far, the literature has reported studies utilizing PVA as a support matrix for electrospinning CMC to produce nanostructured mats for biomedical applications [30–33]. However, there is a lack of studies exploring the optimal PVA grade for producing defect-free electrospun mats. Given the challenges posed by high-degree hydrolyzed PVA, particularly in electrospinning processes, it is essential to address this gap [34]. A comparative study of different PVA grades would be valuable to understand their influence on spinnability when combined with carboxymethyl cellulose (CMC), a biopolymer widely employed in biological applications.

Based on this, the objective of this study was to investigate the reliability of carboxymethyl cellulose (CMC) as an additive in poly(vinyl alcohol) (PVA) for the production of electrospun fibers. Two types of PVA, differing in degree of hydrolysis and molecular weight, were examined to evaluate how these variables influenced fiber formation and morphology. Initially, the PVA was characterized in solution through viscosity and surface tension analyses at different concentrations. The spinning capacity of the PVA solutions, both with and without CMC, was assessed using scanning electron microscopy (SEM). Samples that exhibited the best morphology, defect free, were subjected to composition and thermal stability analyses using FTIR-ATR and TGA/DSC, respectively. This study aimed to establish optimized formulations of PVA/CMC (in an 8:2 ratio) for the production of electrospun mats, with potential applications as bioactive dressings for skin regeneration.

## 2. Materials and Methods

### 2.1. Materials

In this study, two different types of poly(vinyl alcohol) (PVA) were used. The first, PVA.1, was purchased from Sigma—Aldrich (São Paulo, Brazil), with a Mn: 85,000–124,000 g/mol, and a degree of hydrolysis of 99%. The second, PVA.2, was purchased from Vetec—Indústria Química (Rio de Janeiro, Brazil), with an Mn of 60,000–80,000 g/mol, and a degree of hydrolysis of 86.5–89.5%. Sodium carboxymethyl cellulose (CMC) was acquired from Sigma—Aldrich (Rio de Janeiro, Brazil), with an Mn of ~250,000 g/mol and a substitution degree of 0.7.

### 2.2. Solution Preparation

Initially, two solutions of PVA (PVA.1 and PVA.2) were prepared using an oil bath at 80 °C with magnetic stirring for 12 h, followed by cooling to room temperature and subsequent refrigeration. A 100 mL solution of PVA.1 was prepared at 12 wt.% using Milli-Q water as the solvent. Subsequently, three aliquots were prepared and adjusted to 4, 5, and 6 wt.% with a volume of 5 mL taken from the initial 12 wt.% solution. The same method was applied to PVA.2, which was prepared using 100 mL of Milli-Q water as the solvent at the concentration of 16 wt.%. Aliquots of 5 mL from this solution were withdrawn and adjusted with Milli-Q water to obtain concentrations of 6, 8, and 10 wt.% of PVA.2.

For the preparation of the CMC solution, 4 g were weighed and dissolved in 100 mL of Milli-Q water. The solution was prepared with magnetic stirring at room temperature by gradually adding the polymer to avoid the formation of aggregates. After dissolution, the solution was refrigerated at approximately 4 °C.

The PVA/CMC solution was prepared by mixing the aforementioned solutions with magnetic stirring in a volumetric ratio of 8:2, as described by Oliveira et al. (2017), who reported this polymer ratio as the optimal proportion for use in skin dressings [16]. Based on the previous research, the concentrations of PVA and CMC in the final solution were evaluated by performing different mixtures.

### 2.3. Electrospinning Process

In this study, a horizontal electrospinning apparatus was used. It consists of a high-voltage power supply (model PS/FC 60p02.0-1), an injector pump for syringe (KDS series 100), and an aluminum collecting plate connected to the ground. A volume of 5 mL of each solution was loaded into a plastic syringe with an 18-gauge metal needle using 11 cm of the distance tip needle–collector. The solutions were electrospun for a duration of 20 min to observe the influence of variables on fiber morphology. For this, parameters were evaluated as the applied voltages were 15, 17, and 20 kV, and using flow rates of 0.1, 0.5, 0.6, and 1.0 mL/h. Once the electrospinning parameters for the optimal defect-free morphology were selected, the PVA and PVA/CMC solutions were spun for approximately 4 h. The collector was covered with aluminum foil sheets to facilitate the removal and subsequent handling of the produced samples.

### 2.4. Characterization

#### 2.4.1. Viscometry Study

Viscosity analysis of the polymeric solutions of PVA (1 and 2) and PVA/CMC blends, with varying concentration of the polymers, was performed on a ViscoQC-100 rotational viscosimeter (Anton Paar Trading Co., Shanghai, China). The analysis utilized the CC18 spindle and varied the shear rate (1 to 10 rpm) at room temperature.

#### 2.4.2. Surface Tension of Solutions

The surface tension for each solution was evaluated using the drop weight method. For this, a Pasteur pipette was used to 50 drops of each solution, and the weight of the drops was compared with that of distilled water, maintaining a relationship with the surface tension of water (0.72 N/m) [35]. The surface tension ( $\gamma_x$ ) value was calculated using Equation (1):

$$\gamma_x = \frac{\gamma_w \times M_x}{M_d} \quad (1)$$

#### 2.4.3. Morphological Evaluation—SEM

The surface morphology of the electrospun mats was assessed using a Versa 3D Dual Beam—FEI (OR, USA), operating at an acceleration voltage of 15 kV. Prior to analysis, the samples were coated with gold using a Denton Vacuum—Desk V sputter coater (NJ, USA) for 120 s at 30 mA and vacuum of 50 mTorr. Image processing of the obtained images was performed using Size Meter 1.1 software to quantify the fiber diameter (n: 50).

#### 2.4.4. Chemical Composition—(FTIR-ATR)

The composition of the mats and the chemical interaction of the polymers were evaluated using a Fourier Transform Infrared Spectrophotometer PerkinElmer Frontier (Norwalk, USA) with an attenuated total reflectance (ATR) accessory. The analysis was performed in the region of 4000 to 550  $\text{cm}^{-1}$  with 64 scans and a resolution of 4  $\text{cm}^{-1}$ .

#### 2.4.5. Thermal Behavior—(TGA/DTA—DSC)

The thermal stability and weight loss of the neat PVA and PVA/CMC electrospun mats were assessed using thermogravimetry analysis (TGA) with TA TGA Q500 instrument (New Castle, USA), operating with a heating range of 25 °C to 700 °C at a heating rate of 10 °C/min under an  $\text{N}_2$  atmosphere.



The thermal behavior of the samples was investigated using differential scanning calorimetry (DSC) on a Hitachi—DSC 7000 Thermal Analysis system (Japan). Approximately 10 mg of each sample was used in this analysis, conducted at a rate of 10 °C/min under a nitrogen atmosphere with a flow rate of 50 mL/min. The analysis involved two heating cycles, first from 20 °C to 250 °C, followed by a cooling cycle to −20 °C, and then reheating from −20 °C to 250 °C, also at a rate of 10 °C/min under a nitrogen atmosphere with a flow rate of 50 mL/min. The crystallinity degree ( $X_c$ ) was calculated using Equation (2) as follows:

$$X_c = \frac{\Delta H_f}{(1 - w) \times \Delta H_f^0} \times 100 \quad (2)$$

where  $\Delta H_f$  is the melting enthalpy of the endothermic peak of the DSC thermogram (second heating),  $w$  is the PVA concentration (80%), while  $\Delta H_f^0 = 138.6$  J/g is the theoretical melting enthalpy for a 100% crystalline PVA sample [36].

### 3. Results and Discussion

The main objective of this study was to incorporate carboxymethyl cellulose (CMC) into the formulation of dressings, leveraging the advantages this polymer offers for wound regeneration. CMC is known for its excellent exudate absorption capacity, ability to provide moisture to the wound, and antimicrobial properties, among others [3]. These properties could be further enhanced by combining them with the morphological features achieved through electrospinning, resulting in nanofiber mats that resemble the extracellular matrix of the skin and harness the healing properties of CMC [31,37].

However, significant challenges were encountered in electrospinning CMC, categorizing it as an unreliable biopolymer for fiber formation. Various methodologies have been explored to address this issue, including physical and chemical treatments to synthesize a thermoplastic CMC suitable for electrospinning [9]. An alternative approach involves the production of a polymer blend using a second, easily spinnable polymer as a support for CMC fiber formation.

In line with this alternative, PVA was used as a spinning support to reinforce the CMC chains. According to literature records, PVA is widely used in the production of electrospun nanofibers and is capable of generating thinner fibers compared to those achieved with other easily spinnable polymers, such as poly( $\epsilon$ -caprolactone) (PCL). Therefore, a study of the spinning variables for pure PVA was conducted as a preliminary phase before investigating the electrospinning of PVA/CMC, following the variables studied in previous research within our research group.

#### 3.1. PVA and PVA/CMC Solution Characterization

Initially, a viscosity study was conducted to evaluate the behavior of PVA, CMC, and their respective blends as a function of the concentrations of the PVAs used in this research. To achieve this objective, concentrations of PVA.1 and PVA.2 solutions were varied (Figure 1) using ultrapure water (Milli-Q) as a solvent system.

Figure 1 shows the comparative evaluation of two different solutions of PVAs with varying molar masses and degrees of hydrolysis, which are characteristics that influence the polymeric solution. For each PVA, three different concentrations were evaluated, along with the influence of CMC on the PVA solutions, following a mass ratio of PVA to CMC of 8:2. The viscosity and surface tension of PVA solution and their blends were assessed.

Viscosity analysis is crucial for understanding the behavior of PVA and CMC solution during the electrospinning process, as viscosity directly affects fiber formation and morphology [38]. In this study, two PVAs were utilized, differing in molecular weights: PVA.1 (Mn: ~100,000 g/mol, HD: >99%) and PVA.2 (Mn: ~70,000 g/mol, HD: 88%). The viscosities of the solutions were analyzed by varying the concentrations of the polymers: PVA.1 at 4, 6, and 8 wt.%, and PVA.2 at 6, 8, and 10 wt.%.

As shown in Figure 1A,C, the solutions of PVA.2 exhibited higher viscosities compared to those of PVA.1 (Figure 1C), due to the high degree of interactions between the

polymer chains, resulting in increased resistance to flow [39]. As the concentration of PVA increases, viscosity also tends to rise, reaching 325.9 mPa·s for the 8% PVA.1/CMC solution, which facilitates better formation of the Taylor cone during electrospinning, essential for producing finer and more homogeneous fibers.

The solutions of PVA.2, at higher concentrations of 8 and 10 wt. %, also exhibited significant increases in viscosity, reaching 566.8 mPa·s for the 8% PVA.2/CMC solution, as shown in Figure 1C. However, its lower molecular weight may limit the formation of robust interaction networks compared to PVA.1, potentially resulting in inferior stability of the Taylor cone and, consequently, the production of fibers with larger diameters and greater variability.

In addition to viscosity, the surface tension of the solutions plays a fundamental role in the electrospinning process. The surface tension of all solutions was measured and is presented in Figure 1B,D. This parameter is critical, as it influences jet formation during electrospinning; solutions with lower surface tension favor the formation of a more continuous and stable jet [40]. The addition of CMC to the PVA solutions, following a mass ratio of PVA/CMC of 8:2, can significantly impact surface tension. CMC, with its surfactant properties, tends to reduce the surface tension of the solution, allowing for better jet atomization and contributing to the formation of finer and more uniform fibers.

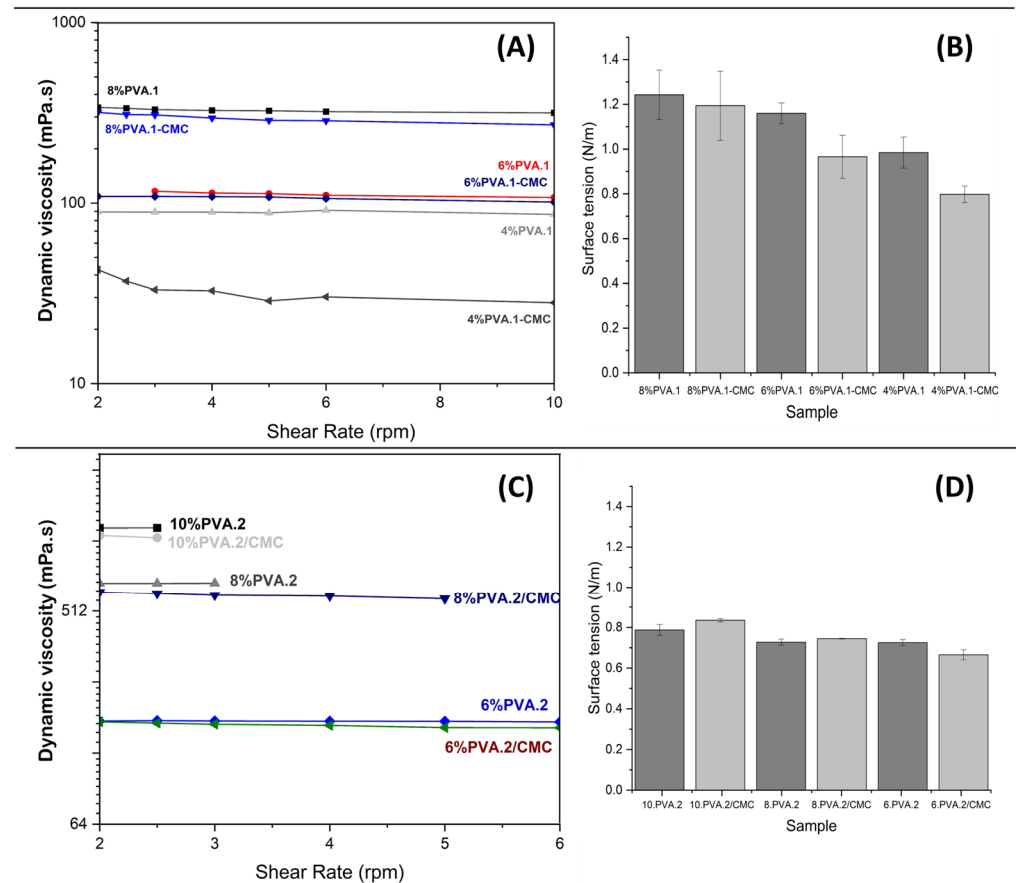


**Figure 1.** Viscosities and surface tensions of PVA and PVA/CMC solutions. For solution from PVA.1 and PVA.1/CMC solutions: (A) viscosity and (B) surface tension. From PVA.2 and PVA.2/CMC solutions: (C) viscosity and (D) surface tension.

The interaction between PVA and CMC may result in a synergy that enhances solution stability; however, it can also complicate the relationship between viscosity, surface tension, and fiber formation. Thus, optimizing these rheological and interfacial properties is fundamental for the success of the electrospinning process.

### 3.2. Morphological Evaluation (SEM)

#### 3.2.1. CMC Spinning Using PVA.1

In the initial phase of this research, the PVA with a molecular weight ( $M_n$ ) of  $\sim 100,000$  g/mol and a hydrolysis degree of 99% was employed. The polymer was solubilized in Milli-Q water (QW). A solution containing 4 wt.% PVA was subjected to electrospinning using previously determined spinning variables. This solution was electrospun along with a 4 wt.% collagen solution, forming the collagen/PVA system, with a collagen/PVA mass ratio of 1:1 [41].

PCL-type I collagen core-shell electrospun nanofibers for wound healing applications was also effectively obtained using acetic acid as solvent [41]. However, the solubility of CMC in acetic acid is poor. For this reason, the electrospinning process in this study utilized an aqueous solvent system with 4 wt.% of PVA.1 in Milli-Q water, varying the rate flow in two points (0.1 and 0.5 mL/h). The electrospun PVA.1 and PVA.1/CMC nanofibers under these variables are shown in Figure 2. The presence of micrometric beads and defects was observed for two flow rates used, while the nanofibers exhibited nanometric diameters. The morphology of electrospun nanofibers is shown, varying the flow rate from 0.1 mL/h to 0.5 mL/h, with average diameters of  $86.8 \text{ nm} \pm 37.1 \text{ nm}$  and  $103 \pm 28.6 \text{ nm}$  observed, respectively, indicating a slight increase in diameter with the presence of defects.

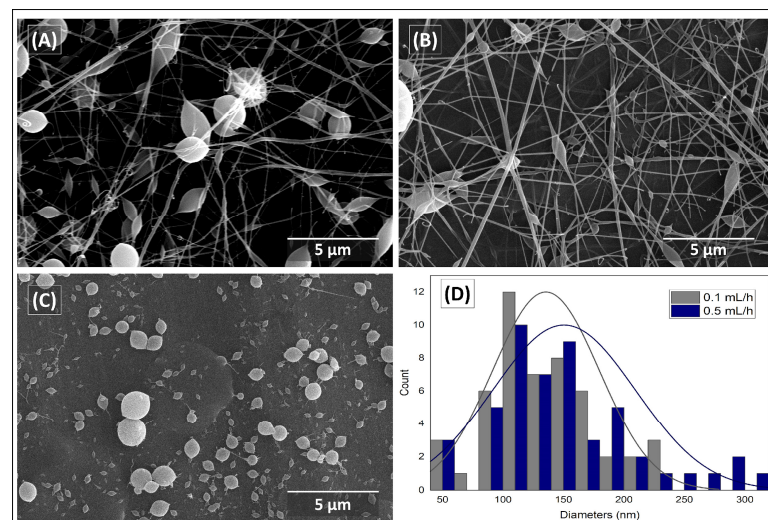


**Figure 2.** SEM images of (4.0 wt. %) PVA.1 nanofiber with rate flow variation. (A) 0.1 mL/h, (B) 0.5 mL/h. PVA.1/CMC: (C) 0.5 mL/h. (D) Histogram of PVA.1 nanofibers.

The images presented in Figure 2 indicate that the polymer concentration used was inadequate, as reflected in the obtained morphology. The presence of the thin fibers with more spherical micrometric beads may be attributed to the low viscosities of the studied solution. Liu et al. (2008) demonstrated that higher polymer concentrations result in a decreased quantity and size of beads produced by electrospinning. Thus, the concentration of 4 wt.% of PVA.1 likely did not exhibit sufficient viscosity for the formation of consistent and fine fibers [42].

Incorporation of CMC into the formulation of PVA.1 at a concentration of 4 wt.% (in an 8:2 mass ratio) altered the morphologies of the nanofibers obtained from neat PVA.1 without CMC (Figure 2A,B) into bead-like morphologies, as shown in Figure 2C ( $\phi = \sim 2.99 \mu\text{m}$ ). This corroborates the difficulty of electrospinning CMC. Figure 2D highlights the morphological variations observed when the polymer flow rate is increased, confirming that an increase in flow rate enhances the distribution of nanofiber diameters. This can primarily be attributed to the increase in the available polymer mass for fiber formation, which consequently creates greater instability in the formation of the Taylor cone.

Two solutions were prepared to continue the electrospinning of PVA.1 in this study: the 6 wt.% PVA.1 solution and PVA.1/CMC (8:2) solution with 6 wt.% PVA. Both samples were electrospun for 20 min using the same parameters. The resulting fibers were characterized by SEM, as shown in Figure 3.

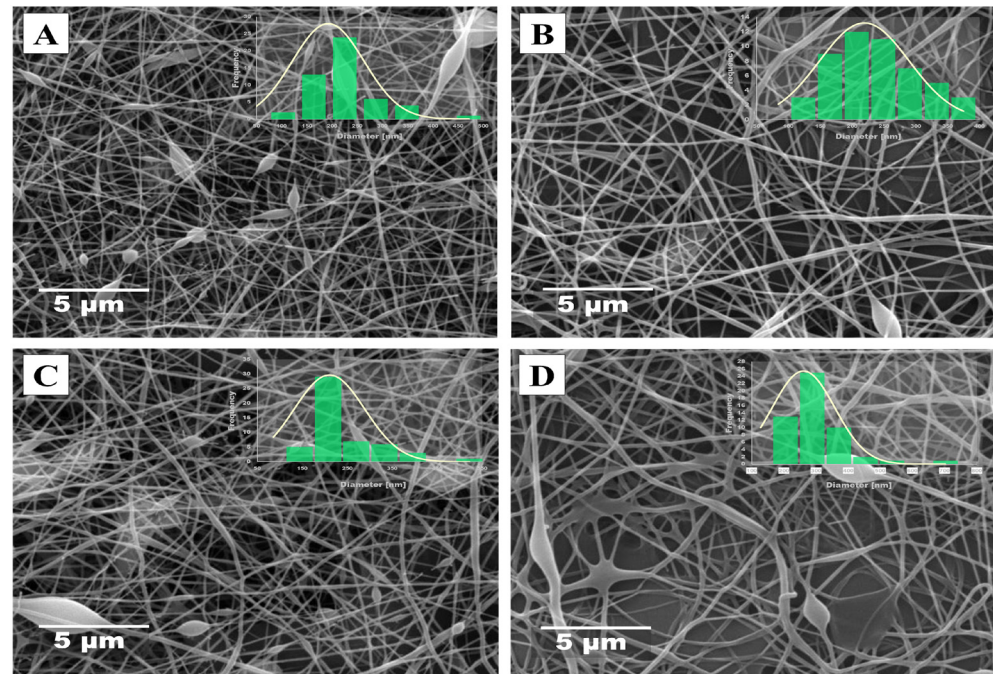


**Figure 3.** SEM images of electrospun nanofibers with 6 wt. % PVA.1 and CMC (8:2 mass ratio). Operating conditions: voltage 17 kV, distance tip needle—collector: 11 cm. Flow rate 0.5 mL/h: (A) Pure PVA.1 and (B) PVA.1/CMC; flow rate 0.6 mL/h: (C) Pure PVA.1, (D) PVA.1/CMC.

Figure 3 shows the morphology of electrospun nanofibers using the same processing conditions for a PVA.1 solution and a PVA.1/CMC blend. The nanofiber diameters for these samples were measured, showing similar morphologies for both electrospinning conditions. In other words, the nanofibers obtained from PVA.1 and PVA.1/CMC did not exhibit significant variations in diameter, with an approximate 14% increase observed for PVA.1/CMC nanofibers compared to neat PVA for the 0.5 mL/h flow rate. The electrospun PVA.1 nanofibers had an average diameter of  $192.3 \pm 71.1$  nm, while PVA.1/CMC nanofibers had an average diameter of  $219.2 \pm 70.3$  nm (Figure 3A,B). This behavior was also observed for nanofibers prepared using the flow rate of 0.6 mL/h, as shown in Figure 3C,D). The variations in the diameter of PVA.1/CMC nanofibers ( $250.2 \pm 74.5$  nm) showed an approximate 22% increase compared to pure PVA.1 nanofibers ( $204.1 \pm 65.5$  nm).

As demonstrated in Figure 1, the incorporation of CMC into PVA.1 solution did not generate significant variations in viscosities; however, nanofibers with larger diameters than those of PVA.1 nanofibers were reflected, as expected. Indeed, an increase in the viscosity of the PVA.1/CMC solution was noted, a characteristic that directly influences the diameters of electrospun nanofibers. The variation in the average nanofiber diameter can be attributed to an increase in the surface tension of the solution due to the presence of CMC, as shown in Figure 1. These characteristics are inherent to CMC in solution, as described in the study by Benchabane and Bekkour (2008), where the rheological properties of neat CMC solutions were investigated [43]. The study revealed that Newtonian viscosity was observed for low concentrations ( $\sim 1\%$  w/v); however, above these values, the solutions began to exhibit rheological properties of thixotropic fluids. This fact could be related to greater difficulties in the production of electrospun nanofibers, explaining the increased defects and agglomerates in the nanofibers. Viscosity and surface tension are crucial variables in the electrospinning process, directly influencing the formation of the Taylor cone, as reported



in the literature [44]. Therefore, the increase in the diameter of PVA.1/CMC nanofibers compared to pure PVA.1 can be attributed to these variations in solution properties.

Thus far, electrospun nanofibers with PVA.1 (4 and 6 wt.%) have generated fine nanofibers on a submicrometric scale. However, all samples have shown defects and beads, with a lower quantity for films obtained with PVA.1 concentrations of 6 wt.%. The result suggests that increasing the concentration provides greater stability to the Taylor cone for the studied variables. However, solutions with this concentration exhibited high viscosity (Figure 1), which also posed greater challenges for processing, ranging from longer solubilization times to instability in PVA.1/CMC solutions.

To assess whether the increase in solution viscosity could generate defect-free nanofibers, electrospinning of PVA.1 and PVA.1/CMC solutions with a mass concentration of 6% relative to PVA.1 was studied. Some of the obtained results are documented in Figure 3, which presents SEM micrographs for two electrospun samples using the same processing variables for PVA.1 solution.

Continuing this study, a PVA.1/CMC solution was electrospun, following the previously described results. For this, variables such as flow rate (1.0 mL/h) and needle tip–collector distance (11 cm) were kept constant. The results are presented in Figure 4, showing the morphological variations of electrospun PVA.1/CMC nanofibers (6 wt.%) using three different applied voltages (15, 17, and 20 kV).

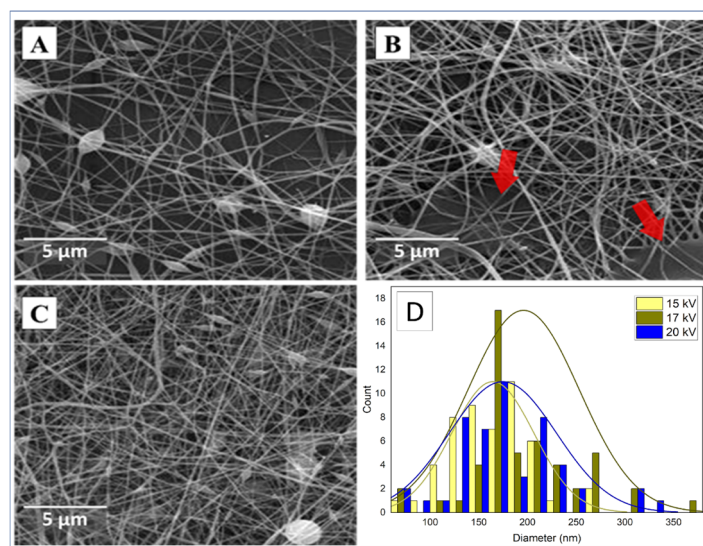


**Figure 4.** SEM images and their histograms for PVA.1/CMC samples with 6% *w/v* (PVA mass ratio). Varying the applied voltage. Operating conditions: 1.0 mL/h, needle tip–collector distance: 11 cm. (A) 15 kV; (B) 17 kV; (C) 20 kV, and (D) histogram comparative.

Under the electrospinning conditions used in this phase of the study, it was observed that voltage variations influenced nanofiber formation (Figure 4). At 15 kV, the presence of large beads is noticeable, which significantly decreases when a voltage of 17 kV is applied, demonstrating a slight improvement in interactions between the polymeric solution and the charges imposed by the applied voltage. This allows electrostatic forces to overcome the surface tension of the solution, enabling the polymer chains to stretch and be ejected at a speed that facilitates the formation of more homogeneous nanofibers. However, some clusters and defects are visible in the micrograph, which may be attributed to insufficient flight time, allowing the deposition of polymeric material still containing solvent. On the other hand, results obtained with 20 kV voltage are consistent with those reported in the literature. Liu et al. (2019) reported that for electrospinning PVA in deionized water, voltages above 20 kV may create instability in the jet and Taylor cone, favoring the formation of multiple jets that induce the formation of coarse defects in nanofiber morphology [45]. However, at this voltage, an improvement in the morphology of electrospun nanofibers



was observed, albeit still with the presence of rounded beads, suggesting that the applied voltage is excessive for the evaluated variables.

In the continuation of the study, solutions with 8 wt. % of PVA.1 and the PVA.1/CMC blend were prepared in aqueous solution (QW), studying voltage variations at 15 and 20 kV for both the PVA.1 and PVA.1/CMC solutions.

In Figure 5, SEM images of electrospun fibers of PVA.1 and PVA.1/CMC are shown as a function of applied voltage. To observe this influence, images with two different magnifications (2k and 10k) are presented to provide a more general view of the produced mats. The solutions used in this part of the investigation had a concentration of 8% *w/v* of PVA.1.

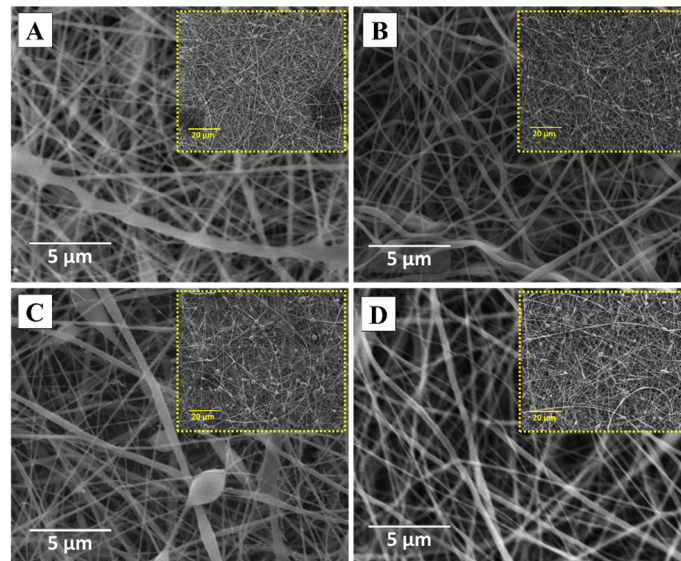


**Figure 5.** SEM images of PVA (8 wt. %) for two magnifications with voltage variation. PVA.1: (A) 15 kV; (B) 20 kV. For PVA.1/CMC solution: (C) 15 kV; (D) 20 kV.

Figure 5A,B illustrate the morphology of PVA.1 nanofibers obtained at 15 kV and 20 kV, respectively, showcasing the production of nanofibers without beads, with average diameters of  $245.9 \pm 96.1$  nm (Figure 5A) and  $217.9 \pm 76.4$  nm (Figure 5B). In these two samples, the formation of beads and/or flattened fibers (ribbons) is the observed morphological characteristic of electrospinning PVA with high viscosity, as described by Koski et al. (2004) [34]. These authors demonstrated that obtaining nanofibers with higher winding or twisting indicates a splitting and spreading of the jet due to Taylor cone instability generated by strong polymer–solvent interaction in viscous PVA/water solutions with a high degree of hydrolysis, which also leads to flattened fibers called ribbons.

Figure 5C,D show the nanofibers produced under the same electrospinning conditions for the PVA.1/CMC solution. The experiment aimed to provide a comparison of morphologies and the effect of CMC incorporation as a function of applied voltage. As shown in Figure 5C, electrospinning the PVA.1/CMC blend resulted in an increase in bead presence when a voltage of 15 kV was applied, compared to the PVA.1 sample (Figure 5A), suggesting a deficiency in the attractive force between the solution and the collector, allowing Taylor cone instability. This behavior was attributed to a possible increase in solution viscosity caused by addition of CMC to PVA, as also observed in Figure 5D, as described by Hashimi et al. (2020). They used polyvinylpyrrolidone (PVP) to reduce solution viscosity, obtaining more stable solutions for use in electrospinning [31].

A study related to the applied flow rate for the PVA.1/CMC solution was conducted. The nanofibers formed by the electrospun samples with this solution are shown in Figure 6, comparing the morphology of PVA.1/CMC nanofibers as a function of the applied flow rate.

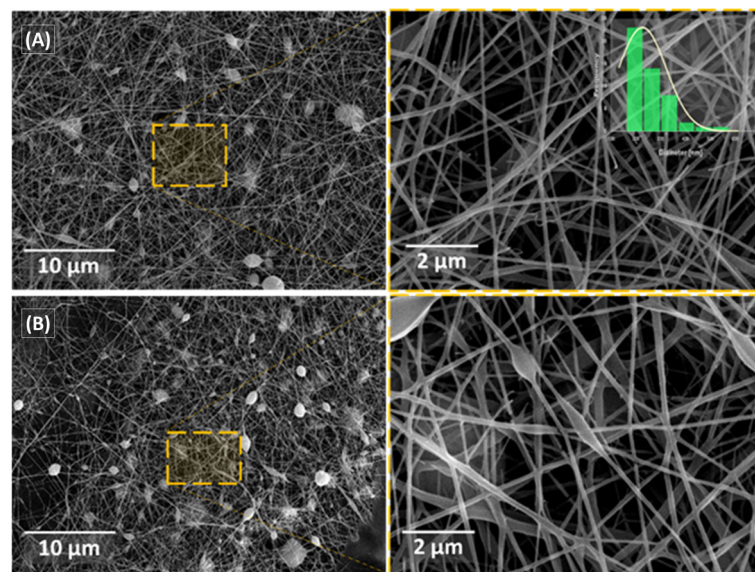


**Figure 6.** SEM images of PVA.1/CMC samples with varying flow rates and different magnifications (voltage: 20 kV; distance: 11 cm) in 5k (**left**) and 20k (**right**). Flow rate: (**A**) 0.6 mL/h and (**B**) 0.5 mL/h.

It was observed that even with a small increase in the flow rate of  $\sim 0.1$  mL/h, the amount of polymeric mass available at the needle tip increased the instability of the Taylor cone, leading to greater bead formation and defects deposited on the collector. This aligns with literature reports indicating that providing a larger amount of polymer requires more force to stretch the available mass, resulting in larger diameter nanofibers and coarser defects. However, the diameters of the produced nanofibers did not show significant variation, measuring  $130.1 \pm 48.0$  nm for the sample with a flow rate of 0.6 mL/h and  $129.9 \pm 78.7$  nm for the sample obtained with a flow rate of 0.5 mL/h. This demonstrates that neither of the two conditions allowed for the defect-free formation of nanofibers with homogeneous diameters. Therefore, it can be concluded that the spinning conditions used for these polymers were not efficient for the formation of fine nanofibers.

As shown in previous studies [41,46], it was observed that this parameter did not influence the electrospinning processing, which could be attributed to instabilities in the Taylor cone resulting from high surface tension of the PVA solution (Figure 1); this result is according to reports in the literature, which show high surface tension for solutions with a high degree of hydrolysis. Some authors who used this same type of PVA (Mn 100,000 and degree of hydrolysis 99%) in electrospinning processes overcame this problem by adding a surfactant to reduce the surface tension of the polymeric solution [18]; however, this is not the focus of this study.

On the other hand, the ease of PVA spinning was studied using a second polymer with a lower degree of hydrolysis (partially hydrolyzed PVA), which are polymers that are easier to solubilize and have lower surface tension. For this second polymer used, the nomenclature PVA.2 was employed, using a PVA polymer with 88% hydrolysis.

### 3.2.2. CMC Spinning Using PVA.2

Similarly, to PVA.1, a study was conducted to investigate variations in PVA concentrations at 6, 8, and 10% (*w/v*), maintaining the volumetric ratio of 8:2 between PVA and CMC. The flow rate was kept constant at 0.5 mL/h, and the applied voltage was the main variable studied.

This phase of the study began with a PVA.2 solution at a mass concentration of 6 wt.%. The morphology of the nanofibers was assessed for this concentration based on the applied voltage. The micrographs obtained in this study are presented in Figure 7.

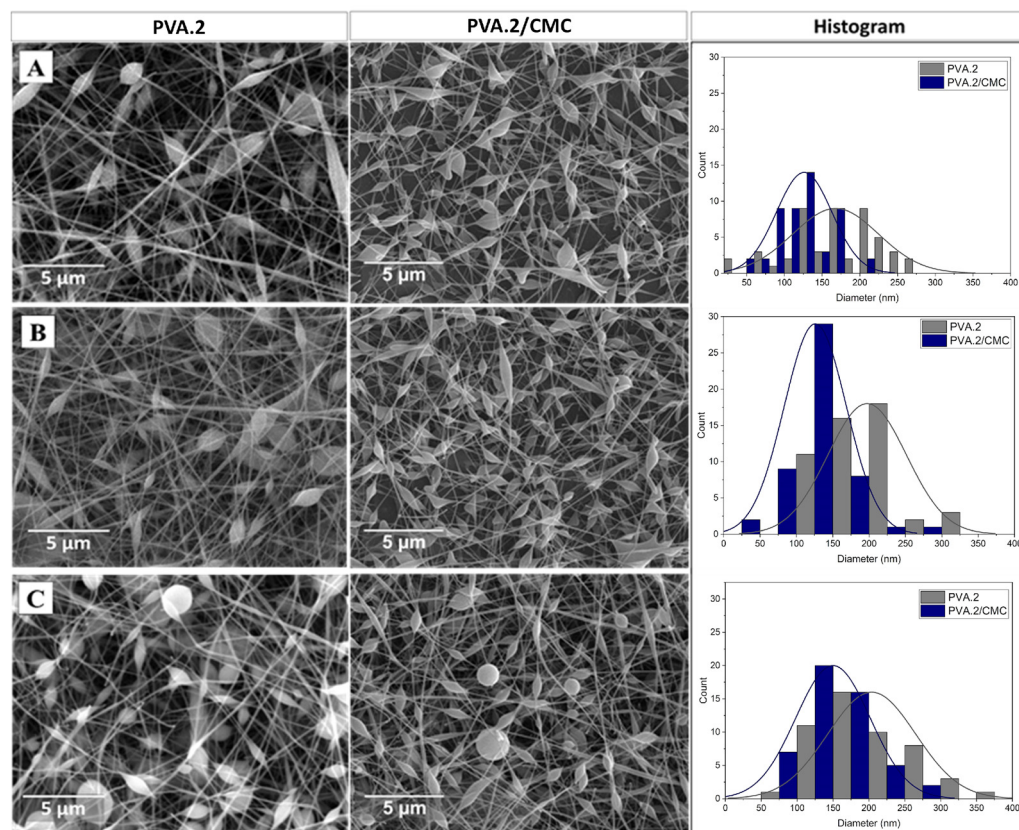


**Figure 7.** SEM images and histograms of PVA.2 (6 wt.%) and PVA.1/CMC (8:2) nanofibers. (A) 15 kV; (B) 17 kV; (C) 20 kV.

Figure 7 shows the morphology of electrospun nanofibers produced from PVA.2 and PVA.2/CMC, starting from a solution with a 6 wt. % mass concentration. However, it is important to note that bead formation at the micrometer scale occurred for all three applied voltages, comparing the micrographs obtained for the PVA.1 under the same processing conditions and concentration. This polymer formed better morphologies compared to the desired ones (nanofibers with smaller defects), related to the lower molecular weight of PVA.2 (Mn: 80,000 g/mol) compared to PVA.1 (Mn: 100,000 g/mol). Thus, in previous studies, it was found that the polymer's molecular weight has a significant influence on processing, as it is directly linked to the viscosity of the spinning solution and the entanglement of polymer chains [47–49]. Therefore, it can be said that these conditions were not favorable for promoting the intertwining of polymer chains, favoring the formation of continuous and defect-free nanofibers [50]. The presence of beads with smaller sizes than those seen in the micrographs for 15 and 17 kV is evident. As reported in the literature, voltages above 20 kV in the electrospinning of PVA create unstable jets over time, promoting defect formation [48].

On the other hand, Figure 7 (center column) shows the nanofibers obtained from the PVA.2 solutions with CMC. It is possible to observe a potential increase in the number of defects and beads, as well as the average diameter of the nanofibers, compared to the mats obtained under the same processing conditions for pure PVA.2 (Figure 7, right column). This may be related to the difficulties in spinning caused by CMC and the instability of the Taylor cone that the PVA.2 solution still experiences due to its low molecular interaction stemming from its low viscosity (Figure 1B). According to the morphology shown in Figure 7, it can be affirmed that the use of solutions with higher concentrations is necessary.

Therefore, the solution concentration was increased to 8 wt. % by mass of solubilized PVA.2 in Milli-Q water. This was used to evaluate the influence of the molecular weight of this polymer, as well as its spinning capability, since PVA.2 also has a lower degree of



hydrolysis. These results are presented in Figure 8, which shows an overall micrograph of the sample to provide a more comprehensive view of the morphology of the produced nanofibers, as well as an image at a higher magnification to facilitate a more detailed view of the nanofibers.

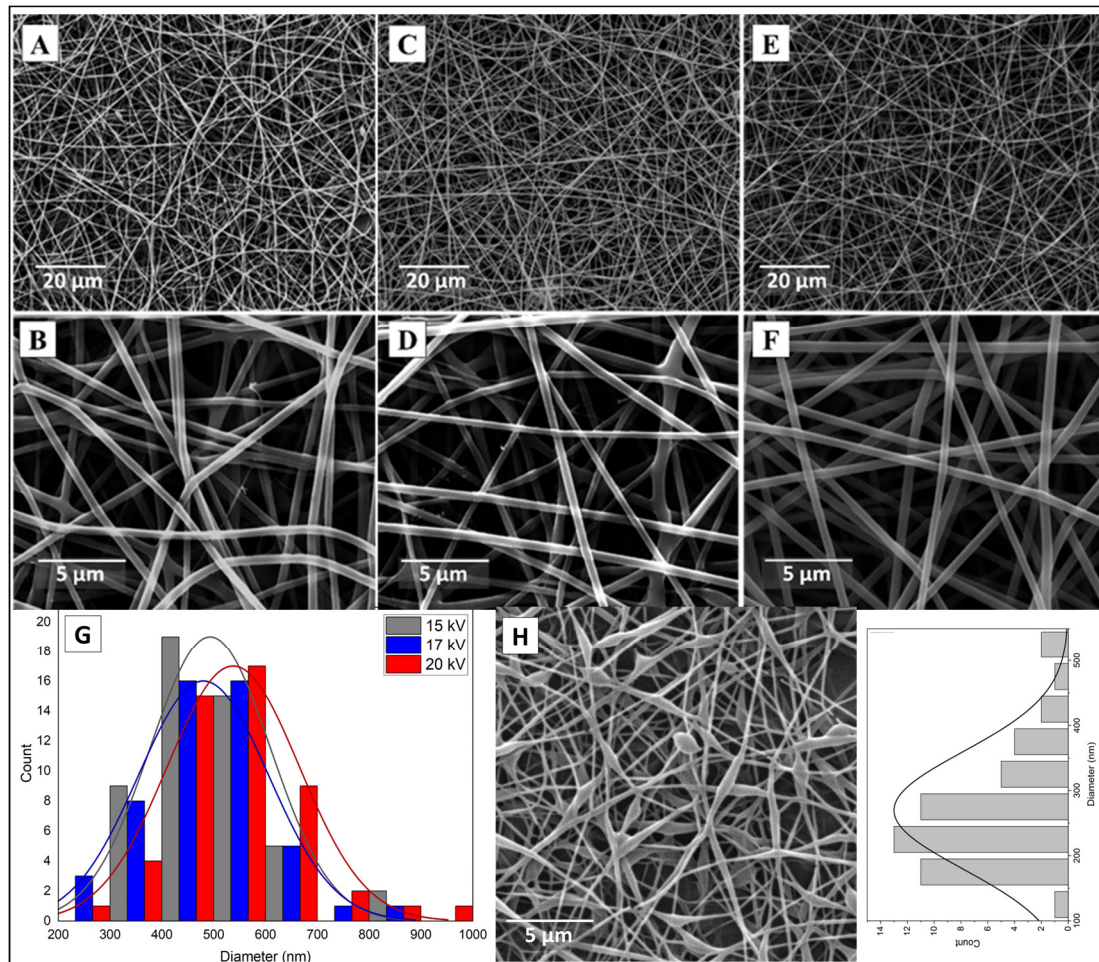


**Figure 8.** SEM images of electrospun nanofibers of 8 wt. % PVA.2 (Mn: 80,000 g/mol), varying the applied voltage at 15 kV (left), 17 kV (center), and 20 kV (right), with two magnifications of 2k (A,C,E) and 10k (B,D,F). (G) Comparative histogram of PVA.2 fibers; (H) PVA.2/CMC fibers and its histogram.

In the micrographs presented in Figure 8, the morphologies of electrospun nanofibers from PVA.2 are shown as a function of the applied voltage. The figure shows that for 8 wt.% PVA.2, the formation of the Taylor cone is stable, which resulted in homogeneous, defect-free nanofibers for all applied voltages (15, 17, and 20 kV), with average diameters of  $466 \pm 104.8$  nm,  $448.6 \pm 117.5$  nm, and  $487.4 \pm 72.5$  nm, respectively. However, the diameters of the nanofibers produced with this polymer are larger than the diameters obtained for PVA.1. The diameters were, however, within the range found in the literature from 100 nm to 2  $\mu$ m. Studies on electrospun PVA report that the higher the molecular weight of the polymer, the larger the diameter of the produced nanofiber when efficient processing parameters are achieved [44,45].

After studying the morphology of the fibers obtained from the PVA.2 (8 wt.%) solution, CMC was added, and the mixture was subjected to electrospinning under the following operational conditions: a flow rate of 0.5 mL/h, an applied voltage of 17 kV, and a distance of 11 cm. Under these parameters, the electrospun sample shown in Figure 8H was obtained. The incorporation of CMC resulted in the formation of defects, as well as a slight reduction

in fiber diameter ( $270 \pm 90$  nm) compared to the average diameter of the sample prepared with pure PVA.2 (Figure 8D). This can be attributed to a lower surface tension of the solution compared to that of PVA.1, which facilitates the formation and stability of the Taylor cone during the spinning process. Furthermore, the negative influence of CMC on the plastic deformation of the solution was evident, potentially leading to the observed defects, which are absent in the neat PVA.2 samples. The viscosity of the solutions for this PVA.2 formulation did not show significant variations, indicating that the presence of defects is merely related to the inclusion of carboxymethyl cellulose.

An additional formulation with 10 wt.% PVA.2 was evaluated to assess the stability of the morphology of the nanofibers produced from a solution with higher concentration and viscosity, following the conditions established for the 8 wt.% PVA.2 solution.

Figure 9 shows the nanofibers obtained from this PVA.2 solution with 10 wt.% mass concentration.

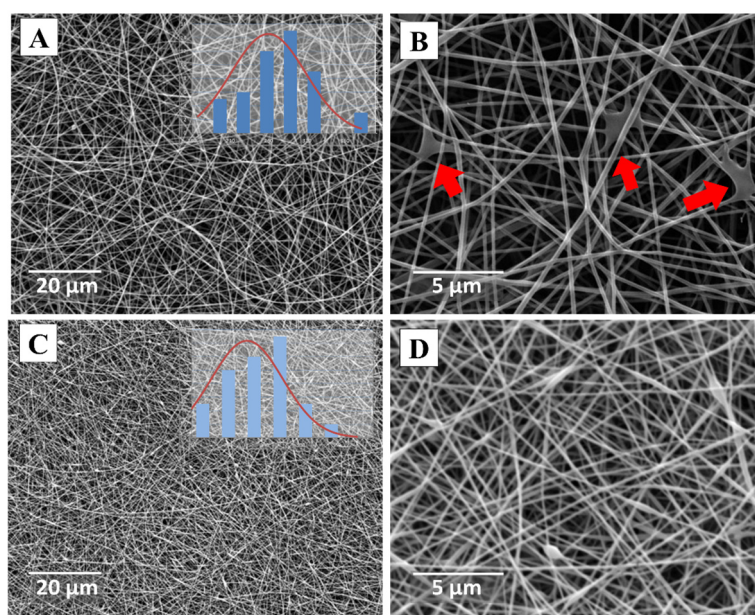


**Figure 9.** SEM micrographs and their histograms for electrospun samples of PVA.2, 10 wt.% (Mn: 80,000 g/mol) with a voltage of 20 kV at two magnifications of 2k (A) and 10k (B), and of PVA.2/CMC (C,D).

Figure 9A shows the SEM image magnified 2k times with its distribution of fibers obtained, with average diameters of  $259.9 \pm 48.9$  nm. This provides a more generalized view of the fiber morphology, showing the presence of nanofibers free from agglomerates and beads. In the micrograph with a magnification of 10,000 times (Figure 9B), it is shown that despite the homogeneity in the diameters of the fibers, defects caused by fiber coalescence can be seen. This effect can be attributed to solvent residues in the fibers that allowed them to fuse when deposited with high humidity from the solvent, creating some agglomerates as highlighted in Figure 9C,D.

Once the electrospinning study of CMC was conducted using two different PVAs as spinning supports, this section presents the SEM micrographs of the selected samples of PVA and PVA/CMC previously studied in this paper. The electrospinning conditions are recorded in Table 1, under which it was possible to obtain mats of nanofibers with minimal defects or none at all.

Once the spinning parameters for the solutions studied in this paper were chosen, the solutions were subjected to electrospinning for 4 h, followed by characterization of the polymers (CMC, PVAs) and their blends (PVA/CMC).



**Table 1.** Summary of electrospinning process conditions for PVA and PVA/CMC (8:2) mats.

Sample	Concentration PVA [wt.%]	Voltage [kV]	Flow Rate [mL/h]	Diameters [nm]
PVA.1	8	20	0.5	217.9 ± 76.4
PVA.1/CMC		20	0.6	129.9 ± 78.7
PVA.2	8	17	0.5	448.6 ± 117.5
PVA.2/CMC	10	20	0.5	270.1 ± 90.6

### 3.3. Chemical Characterization

Figure 10 shows the FTIR spectrum of carboxymethyl cellulose (CMC), revealing several characteristic absorption bands that highlight its chemical structure and functional groups. A prominent and large band is observed at  $3280\text{ cm}^{-1}$ , corresponding to O–H stretching vibrations from hydroxyl groups, which are abundant in CMC and contribute to its hydrophilicity. The spectrum also features a strong absorption band at around  $1584\text{ cm}^{-1}$ , indicative of C=O stretching vibrations associated with carboxyl groups (–COOH), which play a crucial role in the polymer’s reactivity and solubility. Additionally, the C–O stretching vibrations appear in the region of  $1000\text{ to }1200\text{ cm}^{-1}$ , reflecting the ether and alcohol functionalities within the cellulose backbone. Furthermore, bending vibrations of –CH groups are typically seen near  $1414\text{ cm}^{-1}$ , enhancing the overall characterization of the polymer [51,52]. In Figure 11, the spectra of PVA.2 (Figure 11D) also show a band located around  $1733\text{ cm}^{-1}$  corresponding to the C=O stretching vibration, which may indicate the presence of residual acetyl groups, particularly in partially hydrolyzed PVA; these peaks were not observed for PVA.1 (Figure 11C).

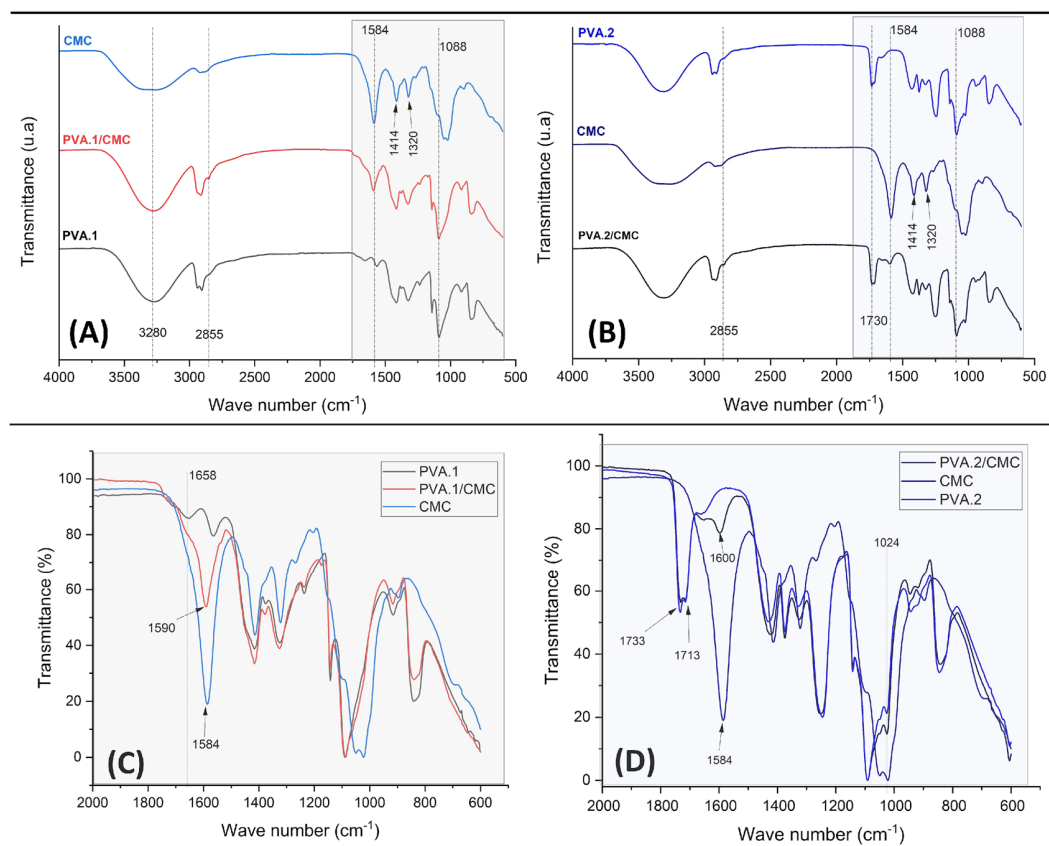


**Figure 10.** Comparative FTIR-ATR spectrograms of PVAs, CMC, and blend electrospun mats. Evaluating for  $4000\text{--}500\text{ cm}^{-1}$ : (A) PVA.1 and PVA.1/CMC mats, (B) PVA.2, and PVA.2/CMC. Zoom of spectrogram in range of  $2000\text{ to }500\text{ cm}^{-1}$ : (C) for PVA.1 and blend mats and (D) for PVA.2 and blend mats.

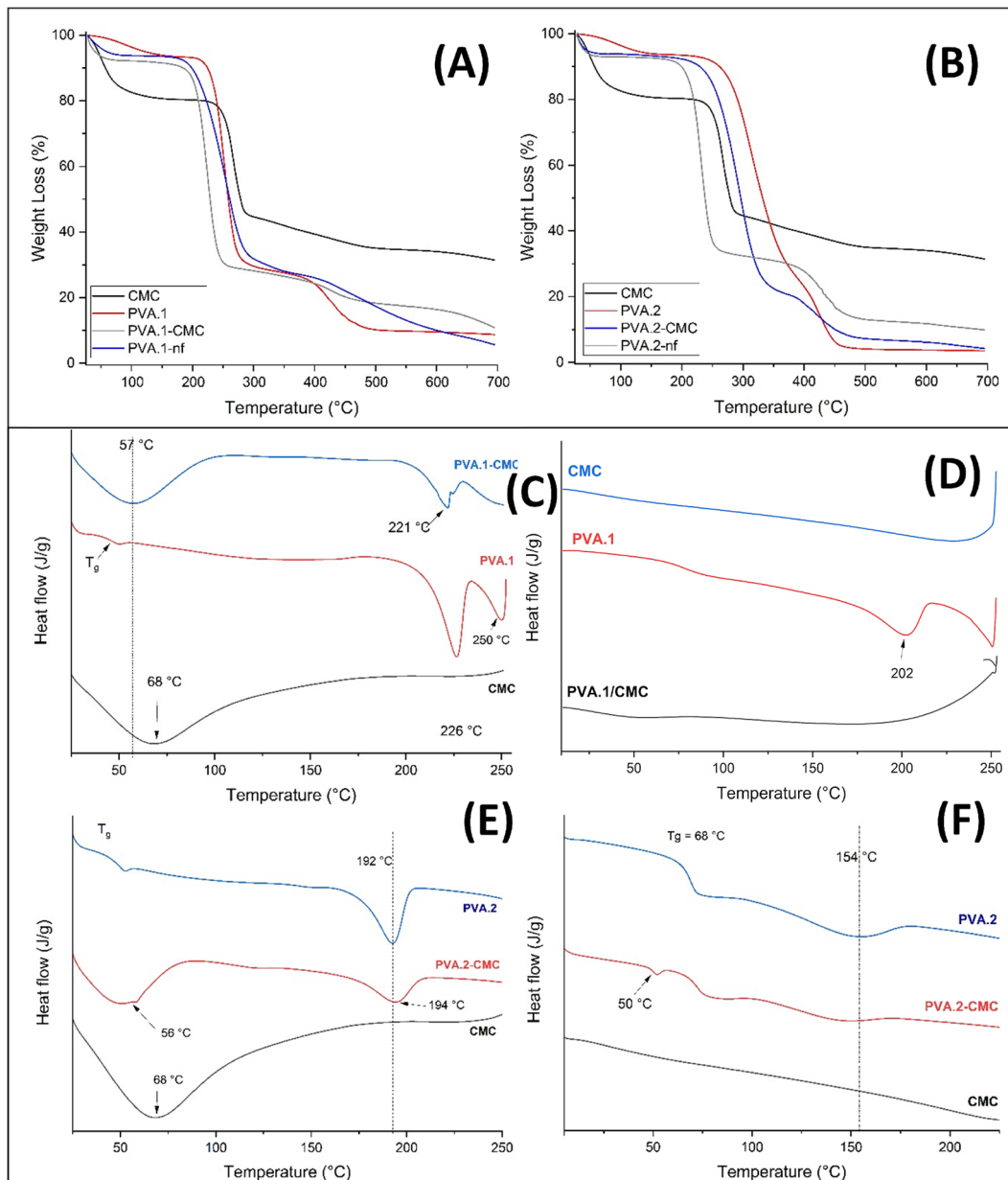


**Figure 11.** TGA and DSC thermograms for different PVAs and PVA/CMC electrospun mats produced by TGA: (A) PVA.1; (B) PVA.2; DSC: PVA.1; (C) first heat cycle; (E) second heat cycle; and PVA.2: (D) first heat cycle; (F) second heat cycle (DSC analysis: Exo up).

Figure 10C,D show that the C–O stretching vibrations are typically found in the range of  $1000$  to  $1300\text{ cm}^{-1}$ , exhibiting multiple peaks that reflect the complexity of the polymer backbone. Furthermore, the bending vibrations of the hydroxyl groups can be observed near  $1400\text{ cm}^{-1}$ . Together, these spectral features provide valuable insights into the chemical properties and functional groups of PVA, influencing its solubility, reactivity, and potential applications [48,50,53].

Finally, the band located at  $1584\text{ cm}^{-1}$  for CMC shifted slightly to approximately  $1600\text{ cm}^{-1}$  in the PVA/CMC blend for both types of PVA, highlighting a possible interaction between CMC and PVA, as evidenced in Figure 10C,D, with the shift of this band to lower wavenumbers below  $1590\text{ cm}^{-1}$ , especially for the PVA.1 samples. This may be attributed to the molecular interactions between the hydroxyl groups on PVA and the carboxymethyl group on CMC [54]. This interaction can be described as a complexation between PVA and CMC, which can lead to changes in the molecular chain structure. According to the

literature, PVA–CMC complexation can be identified by changes in the C–O–C, –COO–, and –OH bands, where shifts or reductions in their wavenumbers and intensities are observed. In Figure 10C,D, a decrease in the intensity of the 1733  $\text{cm}^{-1}$  band (C=O, acetate) confirms the incorporation of CMC into PVA. In addition, Figure 10D shows that a band decreased significantly in the region of 1140  $\text{cm}^{-1}$  for the PVA/CMC blend compared to PVA; this peak is attributed to the crystalline stretching of C=O in the complexation between PVA and CMC. The analysis shows that the complexation reduced crystallinity due to this stretching. This analysis suggests that the complexation process is more favorable for PVA.2, likely due to the residual C=O bonds present in this type of PVA, which has a lower degree of hydrolysis. In contrast, this effect was not observed in the mats produced with PVA.1 (degree of hydrolysis > 99%) in this study [55,56].

### 3.4. Thermal Behavior

The thermal stability of the electrospun mats was evaluated via TGA; the comparative thermograms are shown in Figure 11A for samples produced from PVA.1 and Figure 11B from PVA.2 solution. The thermal transitions of PVA and blends were evaluated using DSC and TGA analysis, and the results are presented in Tables 2 and 3.

**Table 2.** Values of thermal characteristics—TGA of CMC, PVA, and PVA/CMC blended nanofibers electrospun with mass relationship PVAs/CMC of 8:2.

Sample and Degradation Event		T <sub>onset</sub> (°C)	T <sub>max</sub> (°C)	T <sub>endset</sub> (°C)	Mass Loss (%)
CMC	1°	25.0	50.6	251.4	19.9
	2°	251.4	266.6	349.6	40.0
	3°	349.6	429.5	550.5	8.7
PVA.1	1°	214.5	231.4	445.3	60.2
	2°	399.6	430.3	545.1	29.9
PVA.2	1°	214.5	231.4	308.6	60.1
	2°	399.7	430.3	524.9	30.1
PVA.1/CMC	1°	206.1	224.5	389.8	62.4
	2°	398.3	432.1	505.9	16.3
PVA.2/CMC	1°	253.4	292.6	205.1	76.2
	2°	234.8	254.4	347.2	17.7

**Table 3.** Thermal transition evaluated from DSC measurements for CMC, PVAs, and its blended electrospun nanofibers.

Sample	1st Cycle Heat				2nd Cycle Heat				
	T <sub>g</sub> (°C)	T <sub>m</sub> (°C)	ΔH (J/g)	X <sub>c</sub> (%)	T <sub>g</sub> (°C)	ΔH <sub>C</sub> (J/g)	T <sub>m</sub> (°C)	ΔH <sub>m</sub> (°C)	X <sub>c</sub> (%)
CMC	--	--	--	--	--	--	229	29.8	--
PVA.1	47	226.5	47.7	34.4	80	0.07	187.6	17.2	12.4
PVA.1/CMC	--	222.1	17.8	10.3	56	0.33	175.6	13.8	8.0
PVA.2	53	194.0	46.6	33.6	68	0.75	157.6	7.5	5.4
PVA.2/CMC	--	194.1	30.1	17.4	70	0.36	157.3	3.9	2.3

The thermal stability of the CMC, PVA, and PVA/CMC samples was evaluated using thermogravimetric analysis (TGA). For CMC, three thermal events of mass loss were observed, with the first occurring around 50 °C, resulting in an approximate mass loss of 20%. This initial mass loss can be attributed to the moisture present in the CMC molecules, as CMC exhibits hydrocolloid characteristics and has a high capacity for moisture adsorption within its polymer chains. The second event is attributed to the thermal degradation of the CMC chains, resulting in the release of CO<sub>2</sub> [57].

The interaction observed between PVA and CMC is evidenced in Figure 11A,B, where accelerated degradation is noted, reducing the thermal stability of CMC. This is illustrated in Table 2, which shows the presence of two thermal events in the PVA/CMC blends exhibiting a thermal behavior similar to that of PVA, primarily attributed to the higher mass ratio of PVA in the blends. This result corroborates the findings observed via FTIR (Figure 10), where the change in thermal behavior can be attributed to the formation of bonds between the hydroxyl groups of PVA and the carboxymethyl groups of CMC, which influence the structure and thermal stability of the blended mat.

DSC analysis shows the thermal transitions of polymers and blends studied in this research over two heating cycles. The first cycle reflects the thermal history of the electrospinning process, while the second heat cycle shows the characteristic transitions of the samples. Figure 11C,E depict the comparative thermograms of the first heating cycle for the samples related to PVA.1 and PVA.2, respectively. In this analysis, a large peak is observed at approximately 58 °C for the CMC sample, attributed to heat required to vaporize the molecular water present in this biopolymer. Another peak appears in this cycle at around 225 °C for PVA.1 (Figure 11C) and 190 °C for PVA.2 (Figure 11E), corresponding to the melt temperature of PVA crystallites. The second heating cycle is shown in Figure 11D,F. In summary, this thermal behavior is depicted in Table 3, showing that the crystallinity of PVA significantly decreases when its blend with CMC was electrospun, indicating that CMC molecules interfere with the formation of the lamellae of the crystallites. In the first heating for PVA.1 (Figure 11C), three endothermic peaks were observed, attributed to the melting of the crystallites formed during the electrospinning process. These peaks align with those reported in the literature, where the two peaks at temperatures of 221 °C and 250 °C represent the melting of two different populations of PVA crystals, while a smaller peak at 230 °C is associated with the melting temperature of CMC crystals [49,57,58].

#### 4. Conclusions

This study investigated the electrospinning of carboxymethyl cellulose (CMC) when supported in a PVA blend. Two different polymers with varying molar masses and degrees of hydrolysis were examined. It was observed that the surface tension of the spun solutions is one of the most significant variables. Even when using solutions with similar viscosities but different surface tensions, it was found that the solution using PVA.2, which had lower surface tension, produced fibers with more homogeneous diameters and fewer defects compared to the fibers obtained from solutions with a higher degree of hydrolysis (PVA.1). These solution conditions also demonstrated greater ease of electrospinning; however, the mats produced with the PVA.2 solutions exhibited larger fibers ( $\sim 448.6 \pm 117.5$  nm), specifically submicrometric fibers, compared to those produced with PVA.1 ( $\sim 217.9 \pm 76.4$  nm). This behavior was also observed in the composite fibers with CMC (PVA.1/CMC:  $129.9 \pm 78.7$  nm and PVA.2/CMC:  $270.1 \pm 90.6$  nm). However, due to the difficulty in spinning CMC, there was a noticeable loss in the quality of fiber morphology across all PVA/CMC formulations.

The incorporation of CMC into the electrospun PVA samples resulted in reduced crystallinity of PVA at approximately 4% for PVA.1 and 3% for PVA.2, while thermal stability was enhanced in the polymer blends compared to neat PVA. Furthermore, it was observed that these electrospun matrices based on PVA/CMC could serve as drug delivery systems with rapid release due to the hydrocolloid properties conferred by the polymers used in this study. This demonstrates significant potential for their application as dressings for chronic wounds that require moist environments for regeneration.

**Author Contributions:** Conceptualization, J.M.A.-M., M.L.D. and R.M.S.M.T.; methodology, J.M.A.-M., V.F.d.S. and A.Y.B.-L.; validation, J.M.A.-M., V.F.d.S. and A.Y.B.-L.; formal analysis, J.M.A.-M., V.F.d.S. and A.Y.B.-L.; investigation, J.M.A.-M., V.F.d.S. and A.Y.B.-L.; resources, R.M.S.M.T.; data curation, J.M.A.-M., V.F.d.S. and A.Y.B.-L.; writing—original draft preparation, J.M.A.-M.; writing—review and editing, M.L.D. and R.M.S.M.T.; visualization, J.M.A.-M. and A.Y.B.-L.; supervision, M.L.D.

and R.M.S.M.T.; project administration, R.M.S.M.T.; funding acquisition, M.L.D. and R.M.S.M.T. All authors have read and agreed to the published version of the manuscript.

**Funding:** The authors are grateful to the following Brazilian agencies for financial support: Coordenação de Aperfeiçoamento de Pessoal de Nível Superior—CAPES: 001, National Council for Scientific and Technological Development—CNPq (Grants 308789/2020-2, 307364/2018-6, and 312851/2017-0), and Fundação Carlos Chagas Filho de Amparo à Pesquisa do Estado do Rio de Janeiro—FAPERJ (Grants: Rede NanoSaúde—E-26/210.139/2019).

**Data Availability Statement:** The data that support the finding of this study are available from the corresponding authors upon reasonable request.

**Acknowledgments:** The authors are grateful to the Multi-user Microscopy Nucleus of COPPE/Federal University of Rio de Janeiro (Rio de Janeiro, RJ, Brazil) for microscopy analysis, and to the Multi-user laboratory of Material Characterization.

**Conflicts of Interest:** The authors declare no conflicts of interest.

## References

1. Wang, Y.; Xiao, D.; Yu, H.; Zhong, Y.; Zhang, L.; Sui, X.; Wang, B.; Feng, X.; Xu, H.; Mao, Z. Composite hydrogel based oxidated sodium carboxymethyl cellulose and gelatin loaded carboxymethylated cotton fabric for hemostasis and infected wound treatment. *Int. J. Biol. Macromol.* **2023**, *224*, 1382–1394. [[CrossRef](#)] [[PubMed](#)]
2. Pourmadadi, M.; Rahmani, E.; Shamsabadipour, A.; Samadi, A.; Esmaeili, J.; Rahdar, A.; Tavangarian, F.; Pandey, S. Novel carboxymethyl cellulose based nanocomposite: A promising biomaterial for biomedical applications. *Process Biochem.* **2023**, *30*, 211–226. [[CrossRef](#)]
3. Pessanha, F.S.; Oliveira, B.G.R.B.; Oliveira, B.C.; Deutsch, G.; Teixeira, F.; Bokehi, L.C.; Calomino, M.A.; de Castilho, S.R.; Thiré, R.M.S.M.; Teixeira, L.A.; et al. Effectiveness of epidermal growth factor loaded carboxymethylcellulose (EGF-CMC) hydrogel in biofilm formation in wounds of diabetic patients: A randomized clinical trial. *Gel* **2023**, *9*, 117. [[CrossRef](#)]
4. Mansur, A.A.P.; Rodrigues, M.A.; Capanema, N.S.V.; Carvalho, S.M.; Gomes, D.A.; Mansur, S. Functional bioadhesion-enhanced carboxymethyl cellulose/polyvinyl alcohol hybrid hydrogels for chronic wound dressing applications. *RSC Adv.* **2023**, *13*, 13156–13168. [[CrossRef](#)]
5. Isopencu, G.; Deleanu, I.; Busuioc, C.; Oprea, O.; Surdu, V.A.; Bacalum, M.; Stoica, R.; Stoica-Guzun, A. Bacterial cellulose—Carboxymethylcellulose composite loaded with turmeric extract for antimicrobial wound dressing applications. *Int. J. Mol. Sci.* **2023**, *24*, 1719. [[CrossRef](#)]
6. Alsahag, M.; Alisaac, A.; Al-Hazmi, G.A.A.; Pashameah, R.A.; Attar, R.M.S.; Saad, F.A.; El-Metwaly, N.M. Preparation of carboxymethyl cellulose/polyvinyl alcohol wound dressing composite immobilized with anthocyanin extract for colorimetric monitoring of wound healing and prevention of wound infection. *Int. J. Biol. Macromol.* **2023**, *224*, 233–242. [[CrossRef](#)]
7. Xue, J.; Ngadi, M. Effect of methylcellulose, xanthan gum and carboxymethylcellulose on thermal properties of batter systems formulated with different flour combinations. *Food Hydrocolloids* **2009**, *23*, 286–295. [[CrossRef](#)]
8. Biswal, D.R.; Singh, R.P. Characterization of carboxymethyl cellulose and polyacrylamide graft copolymer. *Carbohydr. Polym.* **2004**, *57*, 379–387. [[CrossRef](#)]
9. Lin, X.; Li, Y.; Chen, Z.; Zhang, C.; Luo, X.; Du, X.; Huang, Y. Synthesis, characterization and electrospinning of new thermoplastic carboxymethyl cellulose (TCMC). *Chem. Eng. J.* **2013**, *215–216*, 709–720. [[CrossRef](#)]
10. Yaşar, F.; Toğrul, H.; Arslan, N. Flow properties of cellulose and carboxymethyl cellulose from orange peel. *J. Food Eng.* **2007**, *81*, 187–199. [[CrossRef](#)]
11. El-Newehy, M.H.; El-Naggar, M.E.; Alotaiby, S.; El-Hamshary, H.; Moydeen, M.; Al-Deyab, S. Preparation of biocompatible system based on electrospun CMC/PVA nanofibers as controlled released carrier of diclofenac sodium. *J. Macromol. Sci. A* **2016**, *53*, 566–573. [[CrossRef](#)]
12. Kandasamy, S.; Narayanan, V.; Shanmugam, S. Zinc and manganese substituted hydroxyapatite/CMC/PVP electrospun composite for bone repair applications. *Int. J. Biol. Macromol.* **2020**, *145*, 1018–1030. [[CrossRef](#)] [[PubMed](#)]
13. Alsulami, Q.A.; Alorfi, H.S.; Keshk, S.M.A.S. Thermal stability augmentation of poly(vinyl chloride) by blending with carboxymethyl cellulose. *Polym-Plast. Technol. Mater.* **2022**, *61*, 1719–1727. [[CrossRef](#)]
14. Basu, P.; Repanas, A.; Chatterjee, A.; Glasmacher, B.; NarendraKumar, U.; Manjubala, I. PEO-CMC blend nanofibers fabrication by electrospinning for soft tissue engineering applications. *Mater. Lett.* **2017**, *195*, 10–13. [[CrossRef](#)]
15. Zhang, C.; Wang, R.; Zhang, L.; Liu, Z.; Ning, D.; Li, Q.; Gao, L.; Jiao, T. Self-assembled electrospun PVA/CMC/PEO composite fiber film material with enhanced dye adsorption performance for wastewater treatment. *Colloids Surf. A* **2023**, *678*, 132461. [[CrossRef](#)]
16. Oliveira, R.N.; McGuinness, G.B.; Rouze, R.; Quilty, B.; Cahill, P.; Soares, G.D.A.; Thiré, R.M.S.M. PVA hydrogels loaded with a Brazilian propolis for burn wound healing applications. *J. Appl. Polym. Sci.* **2015**, *132*, 42129. [[CrossRef](#)]
17. Chahardoli, F.; Pourmoslemi, S.; Asl, S.S.; Tamri, P.; Haddadi, R. Preparation of polyvinyl alcohol hydrogel containing chlorogenic acid microspheres and its evaluation for use in skin healing. *J. Biomater. Appl.* **2023**, *37*, 1667–1675. [[CrossRef](#)]



18. Aranha, I.B.; Lucas, E.F. Chemical modification of poly(vinyl alcohol): Evaluation of hydrophilic/lipophilic balance. *Polímeros* **2001**, *11*, 174–181. [[CrossRef](#)]
19. Moraes, I.C.; da Silva, G.G.D.; Carvalho, R.A.; Habitante, A.M.Q.B.; Bergo, P.V.A.; Sobral, P.J.A. Influence of the degree of hydrolysis of poly(vinyl alcohol) on the physical properties of films based on blends of gelatin and poly(vinyl alcohol) plastized with glycerol. *Cienc. Tecnol. Aliment.* **2008**, *28*, 738–745. [[CrossRef](#)]
20. Chiellini, E.; Corti, A.; D'Antone, S.; Solaro, R. Biodegradation of poly (vinyl alcohol) based materials. *Prog. Polym. Sci.* **2003**, *28*, 963–1014. [[CrossRef](#)]
21. Jatoi, A.W.; Jo, Y.K.; Lee, H.; Oh, S.G.; Hwang, D.S.; Khatri, Z.; Cha, H.J.; Kim, I.S. Antibacterial efficacy of poly(vinyl alcohol) composite nanofibers embedded with silver-anchored silica nanoparticles. *J. Biomed. Mater. Res. B Appl. Biomater.* **2018**, *106*, 1121–1128. [[CrossRef](#)]
22. Elhaleem, A.B.A.; Farghali, A.A.; El-Shahawy, A.A.G.; El-Ela, F.I.A.; Eldine, Z.E.; Mahmoud, R.K. Chemisorption and sustained release of cefotaxime and polyvinyl alcohol nanofibers for enhanced efficacy against second degree burn wound infection. *RSC Adv.* **2020**, *10*, 13196. [[CrossRef](#)]
23. Kamoun, E.A.; Chen, X.; Eldin, M.S.M.; Kenawy, E.R.S. Crosslinked poly(vinyl alcohol) hydrogel for wound dressing applications: A review of remarkably blended polymers. *Arb. J. Chem.* **2015**, *8*, 1–14. [[CrossRef](#)]
24. De Souza, B.Z.; Facchi, D.P.; Facchi, S.P.; Teodoro, C.F.; de Almeida, D.A.; Popat, K.C.; Kipper, M.J.; Bonafé, E.G.; Martins, A.F. Electrospun fibers of Ecovio® polymer blends with antimicrobial tea tree essential oil: Enhanced chemical and biological properties. *Processes* **2024**, *12*, 2330. [[CrossRef](#)]
25. Oliveira, R.N.; Meleiro, L.A.C.; Quilty, B.; McGuinness, G.B. Release of natural extracts from PVA and PVA-CMC hydrogel wound dressing: A power law swelling/delivery. *Front. Bioeng. Biotechnol.* **2024**, *12*, 1406336. [[CrossRef](#)]
26. Cacciotti, I.; Ciocci, M.; Di Giovanni, E.; Nanni, F.; Melino, S. Hydrogen sulfide-releasing fibrous membranes: Potential patches for stimulating human stem cells proliferation and viability under oxidative stress. *Int. J. Mol. Sci.* **2018**, *19*, 2368. [[CrossRef](#)]
27. Zhang, X.; Wang, Y.; Gao, Z.; Mao, X.; Cheng, J.; Huang, L.; Tang, J. Advances in wound dressing based on electrospinning nanofibers. *J. Appl. Polym. Sci.* **2024**, *141*, e54746. [[CrossRef](#)]
28. Chen, Y.; Bera, H.; Si, L.; Xiu, F.; Liu, P.; Li, J.; Xu, X.; Zhu, X.; Li, Y.; Cun, D.; et al. Tailor-made curdlan based nanofibrous dressings enable diabetic wound healing. *Carbohydr. Polym.* **2025**, *348*, 122876. [[CrossRef](#)]
29. Maduna, L.; Patnaik, A. Challenges associated with the production of nanofibers. *Processes* **2024**, *12*, 2100. [[CrossRef](#)]
30. Shi, W.; Cai, J.; Yang, Y.; Xu, C.; Lu, J.; Wu, S. Electrospun carboxymethyl cellulose/polyvinyl alcohol nanofiber membranes for enhanced metal ion removal. *Polymers* **2023**, *15*, 11331. [[CrossRef](#)]
31. Hashmi, M.; Ullah, S.; Ullah, A.; Akmal, M.; Saito, Y.; Hussain, N.; Ren, X.; Kim, I.S. Optimized loading of carboxymethyl cellulose (CMC) in tri-component electrospun nanofibers having uniform morphology. *Polymers* **2020**, *12*, 2524. [[CrossRef](#)] [[PubMed](#)]
32. Kazeminava, F.; Javanbakht, S.; Nouri, M.; Adibkia, K.; Ganbarov, K.; Yousefi, M.; Ahmadi, M.; Gholizadeh, P.; Kafil, H.S. Electrospun nanofibers based on carboxymethyl cellulose/polyvinyl alcohol as a potential antimicrobial wound dressing. *Int. J. Biol. Macromol.* **2022**, *214*, 111–119. [[CrossRef](#)] [[PubMed](#)]
33. Hashmi, M.; Ullah, S.; Ullah, A.; Saito, Y.; Haider, K.; Bie, X.; Wada, K.; Kim, I.S. Carboxymethyl cellulose (CMC) based electrospun composite nanofiber mats for food packaging. *Polymers* **2021**, *13*, 302. [[CrossRef](#)] [[PubMed](#)]
34. Koski, A.; Yim, K.; Shivkumar, S. Effect of molecular weight on fibrous PVA produced by electrospinning. *Mater. Lett.* **2004**, *58*, 493–497. [[CrossRef](#)]
35. Teixeira, B.N.; Anaya-Mancipe, J.M.; Thiré, R.M.S.M. Evaluation of polycaprolactone nanofibers' spinnability using green solvent systems by solution blow spinning (SBS). *Nanotechnology* **2023**, *34*, 505707. [[CrossRef](#)]
36. Abazari, M.; Shaarafi, A.; Hassan, M.; Moghimi, H.R.; Andalib, S.; Ghaffari, A. Electrospun silver chloride-loaded PVA nanofibers as a potential antibacterial and electroconductive scaffold for the management of wound infection and healing. *Polym. Bull.* **2024**, *81*, 14921–14956. [[CrossRef](#)]
37. Ergashovich, Y.K.; O'g'li, A.A.A.; Shodievich, A.N.; Ugli, M.M.M.; Sharafovna, R.S.; Jiang, G.; Wan, Y.; Yu, M. Formation, structure, and morphology of nanofiber mat on the base sodium-carboxymethylcellulose/polyvinyl-alcohol/silver nanoparticles composite. *Polym. Adv. Technol.* **2024**, *35*, e6496. [[CrossRef](#)]
38. Wang, H.; Zou, L.; Wang, C.; Li, Y.V. Effect of spinning solution concentration of high DP and high S-diad PVA polymer on the structural properties of high-strength and high-modulus PVA fiber. *Colloids Surf. A Physicochem. Eng. Asp.* **2024**, *701*, 134907. [[CrossRef](#)]
39. Anaya-Mancipe, J.M.; de Figueiredo, A.C.; Rabello, L.G.; Dias, M.L.; Thiré, R.M.S.M. Evaluation of the polycaprolactone hydrolytic degradation in acidic solvent and its influence on the electrospinning process. *J. Appl. Polym. Sci.* **2024**, *141*, e55662. [[CrossRef](#)]
40. De Figueiredo, A.C.; Anaya-Mancipe, J.M.; de Barros, A.O.S.; Santos-Oliveira, R.; Dias, M.L.; Thiré, R.M.S.M. Nanostructured electrospun polycaprolactone-propolis mats composed of different morphologies for potential use in wound healing. *Molecules* **2022**, *27*, 5351. [[CrossRef](#)]
41. Anaya-Mancipe, J.M.; Pereira, L.C.B.; Borchio, P.G.M.; Dias, M.L.; Thiré, R.M.S.M. Novel polycaprolactone (PCL)—Type I collagen core-shell electrospun nanofibers for wound healing applications. *J. Biomed. Mater. Res. B Appl. Biomater.* **2023**, *111*, 366–381. [[CrossRef](#)] [[PubMed](#)]

42. Liu, Y.; He, J.H.; Yu, J.Y.; Zeng, H.M. Controlling numbers and sizes of beads in electrospun nanofibers. *Polym. Int.* **2007**, *57*, 632–636. [[CrossRef](#)]
43. Benchabane, A.; Bekkour, K. Rheological properties of carboxymethyl cellulose (CMC) solutions. *Colloid. Polym. Sci.* **2008**, *286*, 1173–1181. [[CrossRef](#)]
44. Yao, T.; Chen, H.; Samal, P.; Giselbrecht, S.; Baker, M.B.; Moroni, L. Self-assembly of electrospun nanofibers into gradient honeycomb structures. *Mater. Design.* **2019**, *168*, 107614. [[CrossRef](#)]
45. Liu, Z.; Ju, K.; Wang, Z.; Li, W.; Ke, H.; He, J. Electrospun jets number and nanofiber morphology effected by voltage value: Numerical simulation and experimental verification. *Nanoscal Res. Lett.* **2019**, *14*, 310. [[CrossRef](#)]
46. Mancipe, J.M.A.; Dias, M.L.; Thiré, R.M.S.M. Avaliação morfológica de fibras eletrofiadas de policaprolactona em função do tipo de solvente. *Matéria* **2019**, *24*, e12400. [[CrossRef](#)]
47. Mancipe, J.M.A.; Dias, M.L.; Thiré, R.M.S.M. Type I collagen—Poly(vinyl alcohol) electrospun nanofibers: FTIR study of the collagen helical structure preservation. *Polym.-Plastic Technol. Mater.* **2022**, *61*, 846–860. [[CrossRef](#)]
48. Viana, V.R.; Ferreira, W.H.; Azero, E.G.; Dias, M.L.; Andrade, C.T. Optimization of the electrospinning conditions by box-Behnken design to prepare poly(vinyl alcohol)/chitosan crosslinked nanofibers. *J. Mater. Sci. Chem. Eng.* **2020**, *8*, 13–31. [[CrossRef](#)]
49. Vu, T.H.N.; Morozkina, S.N.; Sitnikova, V.E.; Nosenko, T.N.; Olekhovich, R.O.; Uspenskaya, M.V. The influence of acetic acid and ethanol on the fabrication and properties of poly(vinyl alcohol) nanofibers produced by electrospinning. *Polym. Bull.* **2024**, *81*, 9669–9697. [[CrossRef](#)]
50. Ramos, S.P.; da Trindade, L.G.; Mazzo, T.M.; Longo, E.; Bonsanto, F.P.; de Rosso, V.V.; Braga, A.R.C. Electrospinning composites as carriers of natural pigment: Screening of polymeric blends. *Processes* **2022**, *10*, 2737. [[CrossRef](#)]
51. Cuba-Chiem, L.; Huynh, L.; Ralston, J.; Beattie, D.A. In situ film ATR FTIR spectroscopy of carboxymethyl cellulose adsorption on talc: Binding mechanism, pH effects, and adsorption kinetics. *Langmuir* **2008**, *24*, 8036–8044. [[CrossRef](#)] [[PubMed](#)]
52. Sousa, J.P.M.; Oliveira, R.N.; Santos, A.M.N.; Gamallo, O.D.; Araújo, L.S.; Middea, A.; Cid, Y.P.; Castro, R.N. Superabsorbent biodegradable CMC membranes loaded with propolis: Peppas-Sahlin kinetics release. *Polímeros* **2023**, *33*, e20230022. [[CrossRef](#)]
53. Fernandes, I.S.; Saboia, L.C.; Gonçalves, V.S.; da Costa-Neto, J.L.S.; Moreira, A.P.D.; Souza, N.D.; do Nascimento, A.M.; Chaves, D.S.A.; Rosado, L.H.G.; da Silva, L.D.B.; et al. Delivery kinetics of natural active agents by PVA hydrogels intended for wound care. *Matéria* **2023**, *28*, e20230071. [[CrossRef](#)]
54. Nargesi Khoramabadi, H.; Arefian, M.; Hojjati, M.; Tajzad, I.; Mokhtarzade, A.; Mazhar, M.; Jamavari, A. A review of Polyvinyl alcohol/Carboxymethyl cellulose (PVA/CMC) composites for various applications. *J. Compos. Compd.* **2020**, *2*, 69–76. [[CrossRef](#)]
55. Ali, N.S.M.; Zhang, D.; Nagao, Y.; Samsudin, A.S. Molecularly conductive behavior of blended polymer electrolyte-based CMC/PVA. *Makara J. Technol.* **2019**, *23*, 27–31. [[CrossRef](#)]
56. Mohammadkhani, A.; Mohammadkhani, F.; Farhadyar, N.; Sadjadi, M.S.; Kianfar, E. Novel nanocomposite zinc phosphate/polyvinyl alcohol/carboxymethyl cellulose: Synthesis, characterization and investigation of antibacterial and anticorrosive properties. *Case Stud. Chem. Environ. Eng.* **2024**, *9*, 100591. [[CrossRef](#)]
57. El-Sayed, S.; Mahmoud, K.H.; Fatah, A.A.; Hassen, A. DSC, TGA and dielectric properties of carboxymethyl cellulose/polyvinyl alcohol blends. *Phys. B* **2011**, *406*, 4068–4076. [[CrossRef](#)]
58. Fazlina, F.; Hassan, N.A.A.; Fazita, M.R.N.; Leh, C.P.; Kosugi, A.; Arai, T.; Hassan, M.S.; Haafiz, M.K.M. Physicochemical, thermal, and mechanical properties of hemicellulose/carboxymethyl cellulose blend films: The influence of blending composition. *Biomass Conv. Bioref.* **2024**, 1–13. [[CrossRef](#)]

**Disclaimer/Publisher's Note:** The statements, opinions and data contained in all publications are solely those of the individual author(s) and contributor(s) and not of MDPI and/or the editor(s). MDPI and/or the editor(s) disclaim responsibility for any injury to people or property resulting from any ideas, methods, instructions or products referred to in the content.